Multiscale mathematical biology of cell-extracellular matrix interactions during morphogenesis

Rens, E.G.

6

Autocrine Inhibition of Membrane Ruffling Drives Branching Morphogenesis

This chapter is based on:

Rens EG, Zeegers MT, and Merks RMH (2018) *Autocrine Inhibition of Membrane Ruffling Drives Branching Morphogenesis* (in preparation).

Abstract

Branching morphogenesis, the emergence of tree-like structures in organs such as lungs, kidneys and the mammary gland, has been the subject of many *in vitro* and *in silico* experiments. Branching morphogenesis involves many mechanisms, such as cell proliferation, differentiation and migration and is regulated by a network of signaling factors. In this work, we aim to explain how an epithelial tissue can branch autonomously; without cell proliferation and in the absence of signaling from the surrounding mesenchymal tissue. *in vitro* evidence suggests that branching sites are regulated in a curvature dependent manner by an autocrine inhibitory signal that diffuses through the matrix and locally inhibits cell protrusions. Based on this hypothesis, we developed a multiscale cellular Potts model. Using this model, we show that autocrine inhibition of cell protrusions is sufficient to induce branching morphogenesis. The model suggests that the autocrine signal accumulates at concave tissue boundaries, so that cell extensions are more preferable at convex sites. This curvature effect initiates a positive feedback loop where convex sites become even more convex, allowing even more extensions which results in a fully branched structure.

6.1 Introduction

During the development of organs such as lungs, kidneys and the mammary gland, epithelial tissues undergo shape changes during embryonic development resulting in a tree-like structure of branches [275, 276]. The function of branched tissues is to optimize the exchange of chemicals with the surrounding tissue by maximizing its surface. The dynamics of branching from an initially tube shaped epithelial tissue, called the duct, into the surrounding mesenchymal tissue involves involves many cellular mechanisms such as directed cell migration, oriented cell division, cell shape changes, cell differentiation and cell competition (see reviews [277–279]). The specific process of branching morphogenesis varies per organ, but the key mechanisms are believed to be conserved [280, 281]. Although the dynamics of branching in various organs have been characterized well (see for instance, lung: [282], kidney: [283], mammary gland: [284], pancreas [285]), it is still poorly understood what drives branching morphogenesis and which mechanisms are necessary or merely instructive.

For a long time, it was thought that localized cell proliferation is the main driving factor of branching, but more recent experimental data indicate that this is not always true (for review see Ref. [278]). Branches have been observed to initiate and extend prior to the localization of cell proliferation [218, 286]. Signaling factors from the mesenchyme have also been proposed to drive branching [287]. However, the mesenchyme is not required either, as epithelial tissues can branch in the absence of a surrounding mesenchyme *in vitro* [288–290]. In conclusion, it is still poorly understood how epithelial tissues branch autonomously in the absence of cell proliferation and the mesenchyme. Here we propose a cellular mechanism for such autonomous branching of epithelial tissues.

Previous models were often based on tissue growth. They employed known, physical principles of branching growth. It has been thus proposed that epithelial branching can be described by Laplacian growth models. Laplacian growth underlies branching in many non-biological systems, like crystal growth [291] and viscous fingering [292]. In Laplacian growth, the interface of a domain advances with a velocity proportional to the gradient of a field that obeys the Laplacian equation (in quasi-steady state) ($\nabla^2 u = 0$), *i.e.* is dominated by diffusion [293], with $u = 0$ at the interface. Positive curvatures, that arise due to small deviations from a initially homogeneous boundary, experience a higher gradient of the Laplacian field and thus will advance. This curvature effect is then enhanced and the initial deviations advance further. This is known as the Mullins-Sekerka instability that causes branching. In viscous fingering [292], for instance, water is injected into oil between two parallel flat plates. As water is less viscous then oil, the pressure between the two substances makes the water branch out into the oil. It has been proposed that epithelial branching resembles viscous fingering. A mathematical model showed that an epithelial tissue branches into the surrounding mesenchyme if the mesenchyme is less viscous than the luminal fluid in the epithelium [294]. Biological branching has also been proposed to be driven by diffusion limited aggregation (DLA), a concept that is mathematically very similar to Laplacian growth [295]. It was proposed that branching patterns of bacterial colonies are governed by DLA of nutrients [296]. Similarly, it has been suggested that a tumor branches out as proliferating cells consume oxygen [297] and that an epithelial tissue can branch by consuming fibroblastic growth factor (FGF) that upregulates cell proliferation [298].

Other mathematical models proposed that patterns of stimulatory growth factors from the mesenchyme can drive branching by locally upregulated cell proliferation. These models are based on experimental observations that suggest that in the developing lung bud, the position and levels of FGF10 are associated with the mode of branching [299]; domain/lateral branching, planar bifurcation and orthogonal bifurcation [282, 287]. Hirashima *et al.* [300] developed a reaction-diffusion model including FGF10 signaling in the mesenchyme which is inhibited by TGF-β and SHH and activated by SHH. This model suggests that the pattern of FGF10 and thus the mode of branching depends on the curvature of the lung bud, like in Laplacian models. Menshykau *et al.* [301] extended the reaction-diffusion model by including FGF10 induced SHH production in epithelial cells. Furthermore, binding of SHH to its receptor both up-regulates the expression of this receptor and upregulates FGF10 expression in the mesenchyme. During simulated bud growth, the curvature of the domain increases, which causes a localized spot of FGF10 at the tip of the bed. The models suggests that the SHH ligand-receptor interactions allows the localized spots to stabilize. By letting the growth rate of the tissue domain depend on the level of ligand-receptor signaling, it was shown that the tissue branches out [302]. In many branched organs, there are homologies of FGF10 and SSH that drive branching [278] and the ones involved in branching of the kidney have been shown to produce a similar Turing mechanism as in lung [303]. So, it has been suggested that an intricate signaling network between

the epithelium and mesenchyme results in a pattern of growth factors, which drives branching by locally upregulating tissue growth.

Another class of models asked how stereotypic rules for branching splitting determines the architecture of the whole organ. A model that describes branching by chemotaxis towards a growth factor, showed that the number of branches depends on the ratio between the proliferation rate and the chemotaxis speed [304]. Another modeling paper proposed that branch splitting is controlled by an inhibitory signal produced by the epithelium [305]. In this model, it was assumed that a branch bifurcates if the inhibitory signal is below a certain threshold, resulting in a network of branches that avoid each other similar to experimental data [305].

Because there is increasing experimental evidence that inhibitory signals and not stimulatory growth factors are associated with sites of branching [99, 306, 307], mathematical models have explored the role of inhibitory signals. Two different models have suggested that an autocrine signal can drive branching by locally inhibiting tissue growth. One modeling paper argued that the displacement field of a modeled growing domain more accurately fitted to experimental data if an autocrine signal inhibited, instead of stimulated, tissue growth [308]. A cell-based model suggests that a tissue branches due to a curvature effect on an autocrine signal that inhibits cell proliferation [309]. Due to diffusion, the autocrine inhibitor accumulates at concave tissue boundaries, such that cell proliferation occurs at a higher rate at convex tissue boundaries.

Our model is based on *in vitro* observations that suggest a mechanism by which mammary epithelial gland cells can branch out autonomously [99]. In this experimental study by Nelson *et al.* [99] it was asked how branching sites are determined. They embedded mammary epithelial cells in cavities with a specific geometry in 3D collagen gels, to study the extent of sprouting into the surrounding collagen gel. By varying the geometry, it was found that cell protrusions into the surrounding gel were most frequent at sites where the geometry was convex. It was hypothesized that an autocrine signal determines these sites of branching, but it was not known what molecule this could be. A numerical model describing a constant flux of a signal from the tissue (s) and its diffusion (D) and degradation (ϵ) in the matrix ($\frac{\partial c}{\partial t} = D\nabla^2 c - \epsilon c + s$) showed that the autocrine signal accumulated at concave boundaries and that its concentrations negatively correlated with the rate of *in vitro* cell movement. *In vitro* disruption and overexpression of TGF-β caused cell movements to appear or disappear throughout the tissue boundary, respectively. This suggests that TGF-β is responsible for the observed curvature dependent cell movement. Because cell movement and not tissue growth depends on the curvature, this mechanism is conceptually different from Laplacian growth.

We introduce a cellular Potts model to study if such autocrine inhibition of cell movement is sufficient to drive branching morphogenesis. We assume that local concentration of the autocrine signal inhibits cell protrusions at the boundary of the tissue. This model thus suggests that a tissue branches as a result of a curvature effect on cell movement caused by diffusion and degradation of an autocrine signal in the matrix.

In the model the autocrine signal accumulates at concave areas, allowing extensions to occur around the convex areas. Then, the tissue can branch further because tissue extensions at the convex sites makes the tissue more convex (which increases accumulation of the inhibitor at concave areas), making extensions at convex sites even more preferential. The model also suggests that the initiation and speed of branching is regulated by the extent of random motility of cells. Furthermore, the model suggests there is an optimal level of autocrine signaling that promotes branching and that lower surface tensions in our model induces branching.

6.2 Results

Experimental observations suggest that cell protrusions are inhibited by the local concentration of TGF-β [99]. It was hypothesized that diffusion of autocrine TGF-β drives curvature dependent sites of branching [99]. To test if this mechanism suffices to drive epithelial branching, we developed a coupled cell based - continuum model. A framework of this model is given in Figure 6.1. For more details of the model, we refer to the methods section. We model a tissue with the cellular Potts model (CPM) (Figure 6.1A), which describes cells as a collection of lattice sites on a 2D square lattice. So, each lattice site $\vec{x}$ is assigned a spin $\sigma(\vec{x}) \in \mathbb{Z}^{\{0,+\}}$ that describes which cell occupies this lattice site. The spin is assigned value 0 if the medium that surrounds the tissue occupies this site. Cells in the CPM move by making protrusions and retractions. The tissue evolves in time by a Monte Carlo simulation. At each Monte Carlo Step (MCS), a number of N movements are attempted, where N is the number of lattice sites. A movement is defined as copying the spin of a lattice site $\sigma(\vec{x})$ to a neighbouring lattice site $\vec{x}'$. Such a movement is accepted or declined based on a Hamiltonian H that describes the forces acting on the cells:

$$H = \sum_{(\vec{x},\vec{x}')} J(\sigma(\vec{x}), \sigma(\vec{x}'))\mathbf{1}_{\sigma(\vec{x})\neq\sigma(\vec{x}')} + \lambda \sum_{1\leq\sigma\leq n} (a(\sigma) - A_{\text{target}}(\sigma))^2. \tag{6.1}$$

In the first term $(\vec{x}, \vec{x}')$ is a pair of adjacent lattice sites and J the adhesion energy between two lattice sites [1]. The first term approximates a surface tension of the tissue. The second term describes a conservation of cell area. Here, $a(\sigma)$ denotes the area of cell σ and $A_{\text{target}}(\sigma)$ is the target area of cell σ. The parameter λ indicates the strength of this area constraint.

By making a movement, the Hamiltonian of the system changes by ΔH. We assume that the concentration of a diffusive signal inhibits cell protrusions into the surrounding medium. We model this by adding an extra term to the change in the energy (Hamiltonian) of the system:

$$\Delta\hat{H} = \Delta H + \chi \cdot c(\vec{x}') \cdot \mathbf{1}_{\sigma(\vec{x})>0} \cdot \mathbf{1}_{\sigma(\vec{x}')=0} \tag{6.2}$$

[1] The indicator function is defined as $\mathbf{1}_A = \begin{cases} 1 & \text{if } A \text{is true} \\ 0 & \text{if } A \text{is false} \end{cases}$

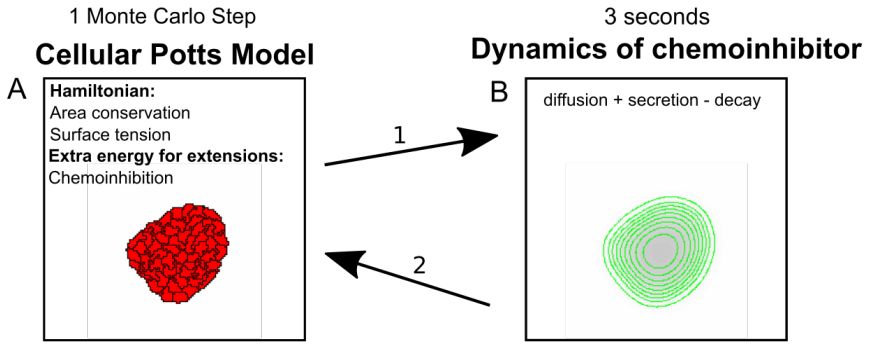

Figure 6.1: Flowchart of the model. (A) CPM calculates cell movement in tissue due to autocrine inhibition; (B) Autocrine signal is forwarded in space and time, according to PDE in Eq. 6.4.

where $c(\vec{x}')$ is the concentration of the inhibitory signal at the protruding site and χ regulates the strength of the inhibition. Now, the total change in energy $\Delta\hat{H}$ determines the probability that a movement is accepted:

$$P(\Delta\hat{H}) = \begin{cases} e^{\frac{-\Delta\hat{H}}{T}} & , \Delta\hat{H} \geq 0 \\ 1 & , \Delta\hat{H} < 0 \end{cases} \tag{6.3}$$

Here T is the cellular temperature, that regulates the extent of random cell motility. The higher the temperature T, the higher the probability a movement will be made against the forces acted on the cell. We assume that the inhibitory signal is secreted by the epithelial tissue and diffuses and decays in the medium (Figure 6.1B). So, we describe the dynamics of the signal by the following partial differential equation:

$$\frac{\partial c(\vec{x},t)}{\partial t} = \underbrace{D\nabla^2 c(\vec{x},t)}_{\text{diffusion}} + \underbrace{\alpha \mathbf{1}_{\sigma(\vec{x})>0}}_{\text{secretion}} - \underbrace{\varepsilon c(\vec{x},t)\mathbf{1}_{\sigma(\vec{x})=0}}_{\text{decay}} \tag{6.4}$$

A simulation consists of consecutive steps of the CPM and the PDE, where one timestep of the CPM is followed by 3 seconds of inhibitor dynamics. This time scale was chosen arbitrarily. Other parameter values are given in Supplementary Table 6.1.

6.2.1 Autocrine inhibition of cell movement drives branching

To study the dynamics of the model, we run the model for 20.000 MCS. The results should give insight in how the tissue morphology progresses over time, as well as why the observed behavior takes place. We initiate approximately 1000 cells, by randomly distributing one-site cells over a disk with radius 0.45 in a tissue of 0.9 mm by 0.9 mm. Then Eden growth [310] is applied for 10 iterations to let the cells grow, thus

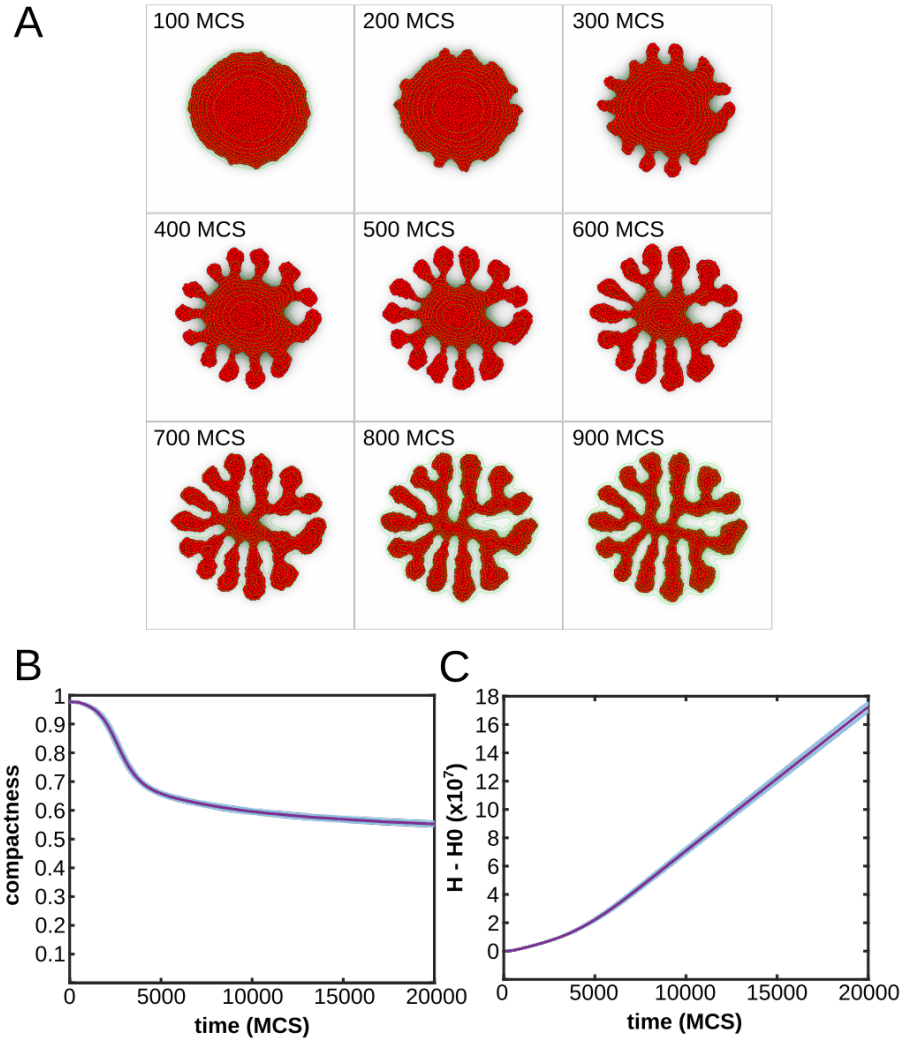

Figure 6.2: Simulation of branching by autocrine inhibition. (A) Timelapse of a model realization; (B) Compactness as a function of time, shaded regions: standard deviations of 100 simulations; (C) Energy spend by the system ($H - H_0 = \sum \Delta H$) as a function of time, shaded regions: standard deviations of 100 simulations.

filling the circular domain. To let the tissue attain a roughly circular shape with cells of similar shape we run the CPM for 100 MCS without the autocrine signal dynamics. Figure 6.2A shows a timelapse of one model realization. A first look at the time series of the simulation shows that at approximately 1000 MCS the boundary of the tissue gets bumpy. Then around 3000 MCS, many droplet-like extensions appear. The length of these extensions increase and as a result, a fully branched structure, with evenly

thick branches is formed, that stabilizes around 8000 MCS.

To quantify the extent of branching, we measured the compactness of the tissue [115] $C = (A_{\text{tissue}}/A_{\text{hull}})$, the ratio between the area of the largest connected component of the tissue and its convex hull, the smallest convex set that contains the tissue [311]. A compactness of 1 implies a perfectly circular tissue shape, whereas a low value of the compactness implies a high degree of branching. Figure 6.2B shows the compactness of the tissue over time. This shows that indeed branching rapidly takes place during the first 5000 MCS and afterwards, the compactness keeps on slowly decreasing, into a stabilized structure.

The behavior of the model can be explained as follows. Initially, due to the random motility of the cells, the boundary of the circular tissue will be become irregular. Consequently, by diffusion, high concentrations of the inhibitor are located at the concave boundaries of the tissue, indicated by the darker grayscales at these locations (see Figure 6.2A), while low concentrations are located at convex boundaries. Because the contribution of the autocrine signal to the change in total energy in the system is always positive, extensions at concave sites are least energetically favourable. Instead, extensions are facilitated at the convex sites of the tissue. As a result, the the boundary at these sites becomes even more convex, allowing for more potential extensions. Thus, this mechanism reinforces itself.

In conclusion, our model suggests that inhibition of cell movement at negative curvatures of the tissue boundary due to autocrine signaling drives a branching instability.

Branching by dissipation

The mechanism in our model resembles a mechanism proposed for vascular network formation of endothelial cells by Merks *et al.* (2008) [115]. Here, it was proposed that cells chemotact towards an autocrine signal and that chemotaxis is contact-inhibited: cells only respond to the signal at cell-medium interfaces. Because cells at the boundary of the tissue experience a shallower gradient at positive curvatures, a branching instability occurs. Branching was enabled if cell retractions and protrusions responded to the signal, but also if only cell protrusions responded to the signal. In the latter case, the cumulative energy of the system $H_{\text{cum}}(t) = H(t) - H(t=0) = \sum_{t_i=0}^{t_i=t} \sum \Delta\hat{H}(t_i)$ increased as a function of time, suggesting that the tissue branches by a dissipative mechanism. This is because $\Delta\hat{H}$ is on average positive, due to the relatively large positive energy contribution of protrusions against the chemoattractant. So, on average, cells make movements that cost energy. The intrinsic random motility of cells allows the tissue to deviate from the optimal configuration. Due to such random fluctuations, the tissue becomes unstable and converges to a state outside of thermal equilibrium. Since H_{cum} does not stabilize in time, it actually costs the system energy to stay in this new equilibrium. Figure 6.2C shows H_{cum} as a function of time in our model. Similar to Merks *et al.*, the energy of the system increases over time, indicating that our simulated tissue also branches by a dissipative mechanism. In our case, this is due to the large positive energy contribution of the autocrine inhibition of cell movement in

$\Delta\hat{H}$ (see equation 6.4). Movements with a positive energy change, against the inhibitor, can only occur if there is sufficient random motility, which is regulated by the cellular temperature T (see equation 6.3).

6.2.2 Random motility regulates branch initiation and branching speed

Because the cellular temperature T regulates the extent of random fluctuations, *i.e.* how much the tissue may deviate from its optimal configuration, we will vary T to study how it affects branching morphogenesis in our model. Figure 6.3A shows the different morphologies of the tissue as a function of T. For low values of T, the tissue does not branch. Starting around $T = 20$, the tissue developed droplet-like extensions. For higher values of T the tissue has branched and the branches are longer and thinner. Figure 6.3B shows the compactness of the tissue as a function of T. This shows that the compactness rapidly decreases for increasing values of T and stabilized at around $T = 20$, reflecting that branching occurs from around $T = 20$.

Because a tissue always starts out with droplet-like extensions that later smooth out, see Figure 6.2A, we investigated how the temperature regulates the speed of branching. Figure 6.3B shows the compactness as a function of time for the various values of T. For low values of T such as $T = 18$ and $T = 20$, the compactness decreases, but it does not reach a low compactness before the end of the simulation. We quantified speed of branching by measuring the time $t(C < 0.8)$ it takes for the tissue to reach a compactness below 0.8 (dashed line in Figure 6.3C. Figure 6.3D plots $t(C < 0.8)$ as a function of the temperature T. This shows that the speed of branching quickly increases when T increases and then saturates.

In conclusion, the temperature regulates both the initiation and the speed of branching. If $T < 18$, no branching takes place. If $T > 18$, branches start to extend but the tissue only develops in a fully branched structure before a certain time point if T is sufficiently high.

6.2.3 Strength of autocrine signal has biphasic effect on branching

The previous section showed that cellular temperature affects branch initiation and speed, but has little effect on the morphology of the tissue. We next studied how the chemoinhibition strength χ, that regulates the extent of inhibition of cell extensions due to the autocrine signal, affects branching morphology. Figure 6.4A shows the resulting morphologies as a function of the chemoinhibition strength χ. Interestingly, branching seems to be have a biphasic dependence on the chemoinhibition strength. For low values of χ, no branching takes places. This is because the impact of the autocrine signal is negligible in the total Hamiltonian of the CPM; there is no preference for low compared to high concentrations of the autocrine signal, hence the tissue retains its circular shape. Increasing the value of χ induces branch formation, as now the difference in levels of the autocrine signal concentration around concave and convex sites, do affect the Hamiltonian. However, by increasing χ even further, branching

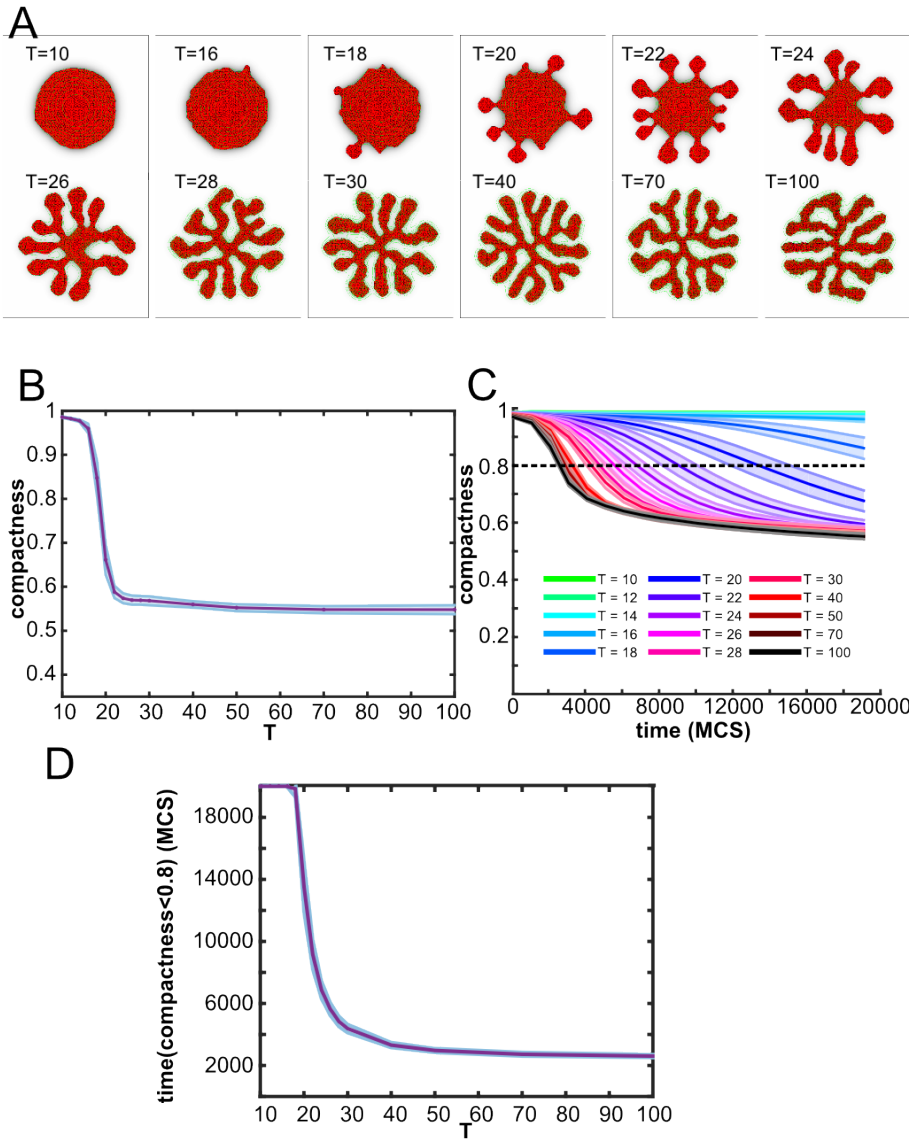

Figure 6.3: Cellular temperature regulates branching dynamics. (A) Example configurations of the tissue at 20000 MCS for different values of T; (B) Compactness as a function of T, shaded regions: standard deviations of 100 simulations; (C) Compactness as a function of time, shaded regions: standard deviations of 100 simulations; different colors: different values for T, see legend.

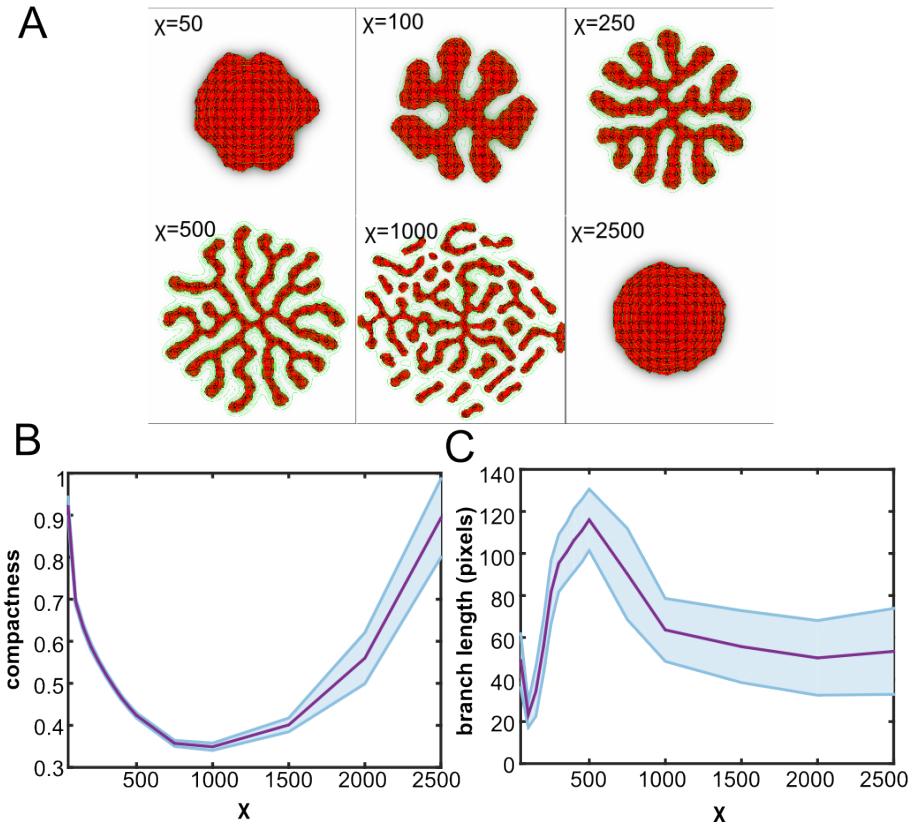

Figure 6.4: Strength of autocrine signal biphasically drives branching. (A) Example configurations of the tissue at 20000 MCS for different values of χ; (B) Compactness as a function of χ, shaded regions: standard deviations of 100 simulations; (C) Branch length as a function of χ, shaded regions: standard deviations of 100 simulations.

occurs at such a fast rate that branches start to break apart from the spheroid, since with high values of χ, the chemoinhibition term in the Hamiltonian starts to dominate over the cell-cell adhesive energy. Then, for more extreme values of χ, branching does not start, because every extension is very costly.

Figure 6.4B shows how the compactness of the tissue depends on the strength of the autocrine signal χ, confirming the biphasic effect of χ. Figure 6.4C shows that χ increases the length of the branches. In conclusion, our model suggests that the autocrine signal regulates the degree of branching in a biphasic manner. A tissue can branch within an optimal range of χ.

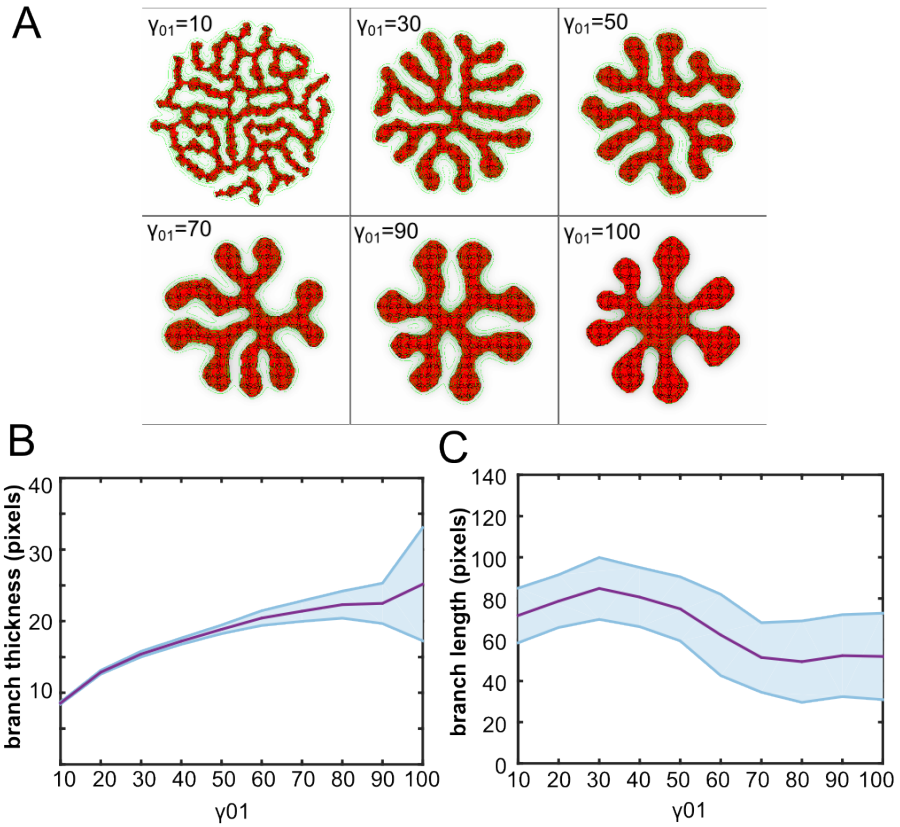

Figure 6.5: Surface tension affects branch morphology. (A) Example configurations of the tissue at 20000 MCS for different values of J_{01}; (B) Branch thickness as a function of γ_{01}, shaded regions: standard deviations of 100 simulations; (C) Branch length as a function of γ_{01}, shaded regions: standard deviations of 100 simulations.

6.2.4 Decreasing surface tension promotes branching

Experimental studies have shown that cytoskeletal tension impacts branching morphogenesis [298, 312, 313]. In the CPM, cytoskeletal tension is associated with the surface tension γ_{01} defined as $\gamma_{01} = J_{01} - \frac{J_{11}}{2}$ [74], where J_{01} is the adhesive energy between cell and medium and J_{11} is the adhesive energy between two cells. Here we will study what effect the surface tension has on the branching morphology in our model, by varying J_{01} and thus γ_{01}.

Figure 6.5A shows the morphologies for different values of γ_{01}. For very low values of γ_{01} there are many thin branches, which seem to have merged, almost resembling a network. Also, the surfaces of the branches are ragged. As γ_{01} increases, the branches become more smooth again and for high values of γ_{01} the branches become droplet-shaped. Figure 6.5B and Figure 6.5C show that decreasing γ_{01} decreases the length and

increases the thickness of the branches. The effect of γ_{01} in our model can be explained as follows. At low values of γ_{01} the energy contribution of chemoinhibition dominates over that of adhesion, so that the tissue is able to branch. Because γ_{01} is low, cell-medium interfaces are allowed, so that branches may elongate and become thin. For high values of γ_{01} it becomes more energetically costly to have a larger cell-medium interface.

Taken together, a decrease in surface tension allows for more cell-medium interfaces so that the tissue is able to deform into a branched structure, with thinner and longer branches.

6.3 Discussion

Using a computational model, we show that inhibition of cell protrusion by an autocrine signal suffices to drive epithelial branching in the absence of cell proliferation and in absence of signaling with the surrounding mesenchyme. In a simulated epithelial spheroid, random cell motility causes the periphery to become bumpy. The tissue branches due to a curvature effect, leading to reduced concentrations of the autocrine signal at convex sites of the tissue boundary. So, cell protrusions are more preferentially at positive curvatures. This results in an instability where local extensions at positive tissue curvature make reinforces the curvature effect so that full branching proceeds (Figure 6.2) that is limited by the surface tension of the tissue.

6.3.1 An autonomous mechanism for branching

Previous mathematical models were often based on Laplacian growth principles, which assume that tissue growth is proportional the gradient of a Laplacian field. In such models, tissues branch due to a Mullins-Sekerka instability, where positive curvatures experience higher gradients of the field and become unstable. It has been proposed that a pressure field between epithelium and mesenchyme [294], or a growth factor field [298, 309] can drive branching. It has also been proposed that patterns of stimulatory growth factors, arising from Turing-type signaling interactions between the epithelium and mesenchyme [300, 301, 303], drive branching by locally up-regulating tissue growth [302, 303]. However, experimental data suggests that branches extend prior to localized cell proliferation [218, 278, 286]. Furthermore, epithelial tissues can branch in absence of the mesenchyme [288–290] and distributions of stimulatory growth factors are not always associated with branch localization [306, 307]. In contrast to previous models, we propose a cellular mechanism for branching and our model suggests that neither tissue growth nor signaling from the mesenchyme is required. Based on experimental data [99], our model suggests that an autocrine inhibitory signal determines sites of branching and drives branching by a curvature effect where the autocrine signal accumulates at concave parts. This curvature effect is similar to curvature effect in Laplacian growth, but our model suggests that curvature dependent cell movement is sufficient to drive branching.

6.3.2 Experimental validation

Autocrine signaling strength

The experimental study on which we based our model suggests that TGF-β acts as the autocrine inhibitory signal [99]. Our model predicts that TGF-β can only drive branching if its signaling strength is around an optimal value (Figure 6.4). In agreement with our model predictions, several experimental studies suggest that TGF-β drives branching in a concentration dependent manner. High concentrations of TGF-β1 to obstructs mammary gland epithelial branching, while low concentrations promoted branching [314]. Furthermore, low concentration of TGF-β promote tubulogenesis in mammary glands *in vitro* [315]. Decreasing the response of TGF-β receptors leads to increased branching [316]. In our model, decreasing χ also increased branching, but decreasing χ even further stopped branching (Figure 6.4). To investigate if the biphasic effect of chemoinhibition strength on branching can be found *in vitro*, it would be interesting to extend the experimental set-up by Nelson *et al.* [99] to larger unconfined mammary epithelial tissues that exhibit full branching morphogenesis (not just sprouting movements) and modulating TGF-β response.

Since many organs have homologies of the TGF-β family and our model does not specify a certain cell type or specific signaling molecule, we may validate our model using experimental observations of various organ systems. In kidney, BMP7 stimulates branching at low concentrations while inhibiting branching at higher concentrations [317]. Similar to our model, the secreted inhibitor is thought to regulate branch avoidance [305]. The shape of the extensions also resembles experimental observations of kidney and lung branches. Initially, the extensions are broad and droplet-shaped, which then elongate over time [283, 298, 318]. In *in vitro* experiments, branch bifurcation occurs very often, which is not the case in our model. Simulations show that if we allow cell proliferation, branch splitting does occur. To better compare *in vitro* branching dynamics with our model in the future, we will generate time evolutions of the skeletal tree of the model configurations, similar to what has been done by Watanabe *et al.* [283]. Directly comparing *in vitro* with *in silico* data could provide us with realistic parameter values, such as the time scale of one MCS. This might alleviate the issue that the current time scale of our model (branching occurs within 2h) is much faster than *in vitro* (2-3 days) [283].

Surface tension

In our model, reducing surface tension promotes branching (Figure 6.5). This compares well with *in vitro* observations by Hartmann and Miura, who showed that disruption of the cytoskeleton in isolated lung epithelium increased branching [298]. Similarly, inhibiting cell contractility promotes branching morphogenesis in pancreas [290]. In contrast with these experiments, increasing cytoskeletal tension in embryonic lung explants increased branching [312, 313]. Because our model is incomplete, *i.e.* it does not involve intricate interplay between lung epithelium, the basement membrane and

the surrounding mesenchyme, and remodeling of the matrix, it can not explain all these experimental observations.

Random motility

In our simulations, the cellular temperature T, that regulates cell motility, promotes branching (Figure 6.3). In agreement with our model, knockout of Btbd7 in kidney increases cell motility, which resulted in less end bends [319]. In these experiments, Btbd7 also decreased cell-cell adhesions. The experimental figures indicate that the buds and branches are thicker [319]. This is also consistent with our model, as an increase in the cell-cell adhesion energy J_{11} is equivalent to a decrease in surface tension γ_{01}, which leads less branches and increased thickness (Figure 6.5).

Our model has given insights into epithelial branching, but it disagrees with observations in kidney. Recent experimental observations suggest that the autocrine inhibitor BMP7 does not regulate curvature dependent protrusion [320]. Using a comparable system to Nelson *et al.* [99], but with renal epithelial cells, Martin *et al.* showed that renal cells did exhibit curvature dependent protrusions, but not because of BMP7 localization. They interfered with autocrine signals, by applying rapid flow to the medium and showed that cells still exhibited curvature dependent protrusions. The authors suggested that this might be regulated by a membrane tension mediated motility instead. The authors also suggest that the mechanism for curvature dependent protrusion could vary among organ systems; mammary cell do use an autocrine inhibitor for this purpose while renal cells do not. Pavlovich *et al.* [306] have argued that reliance of mammary epithelial branching on patterns of inhibitory signals might be unique. So, we might only be able to use our model to gain insights in epithelial branching of mammary gland and not other organs.

6.3.3 Limitations and future work

Like in any model, the model behavior depends on the assumptions that are made. Our model (Figure 6.1) relies on two major assumptions. Firstly, we view the tissue as a cross-section, so that decay of the autocrine signal only takes place outside of the cells. This affects the field of the autocrine signal, which also likely affects the tissue dynamics. Preliminary simulations show that the model also exhibits branching if we allow decay to occur everywhere in the tissue (*i.e.* consider the tissue as a 2D projection). The other major assumption concerns the definition of the Hamiltonian that describes chemoinhibiton of cell movements (Eq. 6.11). Here, cell-matrix extensions are inhibited by the autocrine signal, while cell-cell extensions are independent of the autrocrine signal. As a result, cell copies within the tissue are more often accepted than at the boundary. If we view the tissue as a 2D projection, one could argue that cell-cell copies should also be affected by the autocrine signal, as the cells sense the matrix below them. Therefore, in subsequent research we will investigate the influence of inhibiting extensions at cell-cell copies, similar to Merks *et al.* [115].

The present model greatly simplifies *in vivo* branching, which involves many signaling molecules, from the epithelium and mesenchyme, and their interactions. We could study how interactions between stimulatory and inhibitory growth factors drive branching. Furthermore, signaling molecules such as TGF-β affect different pathways [321] and as such can regulate different types of cell behavior. We could for instance study how growth factor induced patterning of both cell movement and cell proliferation affects branching. The ability of cells to remodel the extracellular matrix has been shown to be involved in branching (for a review, see [278]). For instance, fiber assembly progresses branching in salivary glands [322]. Collagen fiber reorientation directs branch elongation in mammary epithelia [323]. The activity of matrix metalloproteinases (MMPs) has been highly implicated in mammary gland branching [324]. TGF-β is expressed by cells in a latent form that binds to the matrix, and matrix remodeling can release TGF-β from the matrix in an active form [325]. TGF-β can be released from the matrix in many ways (review [321]), for instance due to stretching of latent TGF-β [326]. On stiffer matrices, bound TGF-β experiences more stress, which induces its release [326]. Sites of branching are correlated with matrix stresses [327] and since many morphogenetic processes are highly influenced by matrix stiffness, it would be interesting to implement such interactions between matrix stresses and TGF-β into account.

In summary, we propose that an inhibitory autocrine signal can drive branching morphogenesis by locally inhibiting cell movement. In this model, the autocrine signal accumulates at concave areas, so that branching is reinforced at sites with higher curvature. This work paves the way for studying the effects of cell-cell signaling and other cellular level dynamics on branching morphogenesis.

6.4 Methods

We developed a combined continuum - cell based model to describe the secretion and diffusion of an autocrine growth factor that we assume to inhibit cell movement. The cellular Potts model (CPM) is used to describe cell movement within a tissue composed of discrete cells. The dynamics of the inhibitor are described by a PDE, of which the local concentration feeds back to the CPM by inhibiting pseudopods.

6.4.1 Cellular Potts Model

To simulate collective cell behaviour we use the Cellular Potts model (CPM)[73, 74]. The CPM defines a two-dimensional lattice $\Lambda \subset \mathbb{Z}^2$. The size of the lattice is determined by m and n, which denote the number of lattice sites in the vertical and horizontal axis respectively. The cells are represented as clusters of connected lattice sites. Every site is assigned a value $\sigma(\vec{x}) \in \mathbb{Z}^{\{0,+\}}$, which is called a spin, to identify the cell it belongs to. Spin $\sigma(\vec{x}) = 0$ is reserved for the ECM. Thus, a cell is defined as the set of

lattice sites mapping to the same spin:

$$C(i) = \{\vec{x} \in \Lambda \mid \sigma(\vec{x}) = i\}. \tag{6.5}$$

The CPM uses a modified Metropolis Monte-Carlo algorithm to simulate cell movement. In this Monte Carlo algorithm, Monte Carlo Steps (MCSs) are taken. In one MCS, the CPM attempts N movements, where $N = mn$ is the number of lattice sites. Each movement is defined as follows. A random lattice site $\vec{x}$ is selected. Then, a random site $\vec{x}'$ in the Von Neumann neighbourhood of $\vec{x}$ is selected and the spin $\sigma(\vec{x})$ is attempted to be copied to $\vec{x}'$. The success of this copy depends the change of energy associated with this movement. A Hamiltonian function H represents the total energy of the system, reflecting the forces that are present in the system. The system aims to minimize H. In the simplest version of the CPM the Hamiltonian includes adhesion energies of cell-cell interfaces and area constraints [73]. The Hamiltonian is usually defined as follows:

$$H = H_{\text{adhesion}} + H_{\text{area}} \tag{6.6}$$

$$= \sum_{(\vec{x},\vec{x}')} J(\sigma(\vec{x}), \sigma(\vec{x}'))\mathbf{1}_{\sigma(\vec{x})\neq\sigma(\vec{x}')} + \lambda \sum_{1\leq\sigma\leq n} (a(\sigma) - A_{\text{target}}(\sigma))^2. \tag{6.7}$$

with $(\vec{x}, \vec{x}')$ a pair of adjacent lattice sites. Here J is a matrix with adhesion energies between cell types (ECM and epithelial cells) and δ is the Kronecker delta function ensuring that only cell boundaries are considered in the adhesion summation. In addition, $a(\sigma)$ denotes the current number of sites occupied by cell σ while $A_{\text{target}}(\sigma)$ is the target area of cell σ. The parameter λ indicates the strength of this area constraint. The difference in energy corresponding to a copy is given by:

$$\Delta H = H_{\text{after}} - H_{\text{before}}. \tag{6.8}$$

This difference determines the probability that the copy is accepted. If ΔH is negative, the movement will be accepted, since it will decrease the energy of the system. However, if ΔH is positive, the movement will be accepted according to a Boltzmann distribution, yielding:

$$P(\Delta H) = \begin{cases} e^{\frac{-\Delta H}{T}} & , \Delta H \geq 0, \\ 1 & , \Delta H < 0. \end{cases} \tag{6.9}$$

Here T is the cellular temperature, that regulates the magnitude of intrinsic random cell motility.

6.4.2 Dynamics of autocrine signal

We assume that cells secrete an inhibitor which diffuses and degrades in the ECM, giving rise to:

$$\frac{\partial c(\vec{x}, t)}{\partial t} = D\nabla^2 c(\vec{x}, t) + \alpha \mathbf{1}_{\sigma(\vec{x})>0} - \varepsilon c(\vec{x}, t)\mathbf{1}_{\sigma(\vec{x})=0} \tag{6.10}$$

In this equation $c(\vec{x}, t)$ is the concentration of the chemical at time t and site $\vec{x}$. The PDE contains three parameters, where D is the diffusion coefficient, α is the secretion rate and ε is the decay rate. We view the tissue as a cross-section, and assume decay of the autocrine signal in the medium as it binds to matrix components. Initially there is no signal in the system, thus $c(\vec{x}, 0) = 0$ for all $\vec{x}$. The boundary of the CPM grid acts as a sink, setting $c(\vec{x}, t) = 0$. The PDE is solved by using a forward Euler PDE solver with $h = \Delta x = \Delta y$ being the distance between the lattice site centers, where Δx and Δy are the horizontal and vertical distances respectively. We set Δt to 0.2 seconds and during each Monte Carlo iteration 15 of the numerical integration steps are performed, so that the autocrine dynamics run for $t_c = 3$ seconds.

6.4.3 Local concentration of autocrine inhibits cell movement

To model the inhibitory effect of the autocrine c on the motility of cells, the concentration of the autocrine inhibitor feeds back to the CPM. We assume that, as experimentally observed by Nelson *et al.* [99], inhibition depends on the amount of local autrocrine. In accordance, we extend the expression for ΔH by an additional term:

$$\Delta H_{\text{inhibition}} = \chi \cdot c(\vec{x}') \cdot \mathbf{1}_{\sigma(\vec{x})>0} \cdot \mathbf{1}_{\sigma(\vec{x}')=0} \tag{6.11}$$

The idea of adding this term is that copies toward high concentrations lead to an increase in energy and thus are unfavored. Here, χ, is a parameter that regulates the strength of this inhibition term. The last two terms ensure that this chemoinhibition term comes into play only when a copy is made from a cell to the ECM, modeling a pseudopod extension at the boundary of the tissue.

6.4.4 Morphological measures

We introduce the following morphological measures.

Compactness

The compactness is defined as the ratio between A, the domain covered by the tissue, and the area of its convex hull $A_{\text{convex hull}}$ [311]:

$$C_{\text{comp}} = \frac{A_{\text{tisse}}}{A_{\text{convex hull}}} \tag{6.12}$$

The convex hull of A is the smallest convex set that contains A. The convex hull is determined by first finding the largest connected component [328] and then running Graham's scan [311] to identify the set of points that make up the convex hull. In the context of our simulations, a compactness of $C_{\text{comp}} = 1$ implies a perfectly circular tissue shape, whereas a low value of the compactness implies a high the degree of branching.

Branch length

In order to find the branches of the structure, we generate the morphological skeleton of the tissue [329, 330]. Using this skeleton image, we calculate the length of the branches as follows. For every edge, the two nodes of the edge are removed from the skeleton image A_{skeleton} by removing all lattice sites around the nodes with increasing radius, until a radius w is found such that A_{skeleton} is divided in at least two separate components, of which one is the edge of interest. The length of branch is then determined by counting the pixels that make up the branch and adding twice the radius w to the final result.

Branch thickness

To calculate the branch thickness, we adopted an approach by Filatov *et al.* [331]. We take A to be the image of the tissue and let B be a disk $B^r = \{(x, y) \in \mathbb{R}^2 : x^2 + y^2 \leq r\}$ with variable radius r. The branch thickness can now be defined as the value of r for which branches disappear out of the morphological opening $A \circ B^r$. According to the graph in Figure 6.6 the area of the morphological closing decreases exponentially with the radius r, because more branches disappear from the image with increasing r. We approximate the branch thickness by finding a point where this graph decreases sufficiently fast and then becomes flat, indicating that most branches have disappeared. For more details, see the Supplementary Methods.

6.5 Supplementary methods

6.5.1 Calculating branch thickness

According to the graph in Supplementary Figure 6.6 the area of the morphological opening $A \circ B^r$ decreases exponentially with the radius r. At some point the graph is more or less horizontal. This region corresponds to the circular part of the tissue, in which many circles B^r fit. So, the value for r for which the graph becomes horizontal indicates is the thickness of the branches. We detect this horizontal region by first finding a region where the graph decreases sufficiently fast and then a region where it decreases slow. Let $M_A(r)$ be the area of $A \circ B^r$. We find an $0 < r_1 \leq r_{\max}$ for which $M_A(r_1) - M_A(r_1 - 1) < a_1$ and then the value $r_1 < r_2 \leq r_{\max}$ for which $M_A(r_2) - M_A(r_2 - 1) > a_2$ (r_2 is set to $r_{\max}$ if such a value does not exist). The branch thickness is then found by taking the value of r for which $M_A(r)$ is closest to $\frac{1}{2}(M_A(0) + M_A(r_2 - 1))$. The values of a_1 and a_2 are experimentally determined. The value of $r_{\max}$ is set to 30 to reduce computation time.

In case of no branches or very small branches ($M_A(r_1) - M_A(r_1 - 1) \geq a_1$ for all $0 < r_1 \leq r_{\max}$) we apply the following algorithm. When the decrease in $M_A(r)$ is not larger than $-a_1$ in the entire graph we simply take the distance from the center of mass of the tissue to an ECM point in four different directions and select the lowest distance as the radius. In this case, the radius represents the radius of the unbranched cell aggregate but we take this as the branch thickness. We take this approach since increasing the radius to the width of the initial circular tissue (typically more than twice as large as $r_{\max} = 30$) and repeatedly computing $M_A(r)$ requires a lot of computation time.

6.6 Supplementary tables

Parameter	Description	Value	Unit	value was
T	Cellular temperature	50	-	similar to [115]
A_σ	Target area	50	-	similar to [115]
χ	Chemoinhibition parameter	250	$\frac{Nm}{molL^{-1}}$	chosen
λ	Area constraint strength	50	$\frac{N}{\mu m^3}$	similar to [115]
D	Diffusion coefficient	$15 \cdot 10^{-13}$	$\mu m^2 s^{-1}$	similar to [115]
ε	Decay rate	0.005	s^{-1}	similar to [115]
α	Secretion rate	0.0005	s^{-1}	similar to [115]
$n_{\text{init cells}}$	Number of initial cells	1000	-	chosen
J_{01}	Cell-ECM adhesion energy	50	Nm	similar to [115]
J_{11}	Cell-Cell adhesion energy	20	Nm	similar to [115]
dt	Timestep in PDE integrator	0.2	s	similar to [115]
dx	Pixel size	$2 \cdot 10^{-6}$	m	chosen
P	PDE iterations per MCS	15	-	similar to [115]
m	Vertical size of field	450	-	chosen
n	Horizontal size of field	450	-	chosen

Table 6.1: Parameter settings.

6.7 Supplementary figures

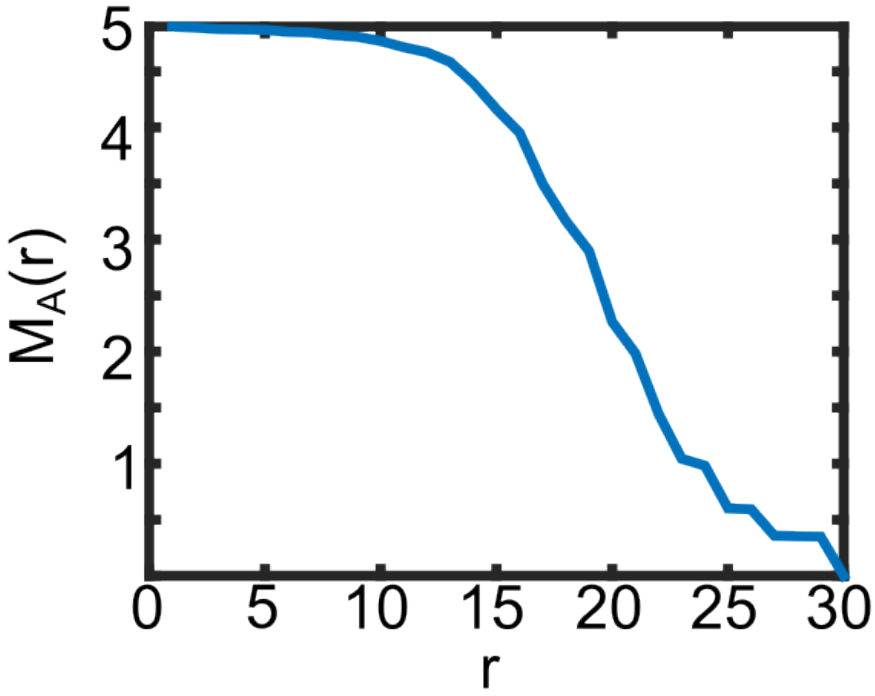

Figure 6.6: The radius *r* versus the area of the morphological closing.